Lifetime measurements of the first 2^+ states in ^{116,118}Te

C. B. Li,[1,*] Y. Zheng,[1] T. X. Li,[1] X. G. Wu,[1] H. Y. Wu,[1] M. Zheng,[1] Z. H. Zhao,[1,2] Y. Q. Li,[1] R. Hong,[1,3] Z. Y. He,[1] J. Z. Li,[1] J. L. Wang,[1] C. Y. Guo,[4] Z. X. Zhou,[4] L. Ni,[4] G. S. Li,[5] X. H. Zhou,[5] B. Guo,[1] S. Y. Wang,[6] M. L. Liu,[5] Y. H. Zhang,[5] C. Y. He,[1] F. L. Liu,[1] S. Wang,[6] and L. H. Zhu[7]

[1]*China Institute of Atomic Energy, Beijing 102413, China*
[2]*Department of Physics, Jilin University, Changchun 130023, China*
[3]*Department of Science, Xihua University, Chengdu 610039, China*
[4]*State Key Laboratory of Nuclear Physics and Technology, Department of Physics, Peking University, Beijing 100091, China*
[5]*Institute of Modern Physics, Chinese Academy of Sciences, Lanzhou 730000, China*
[6]*Department of Physics, Shandong University (Weihai), Weihai 264209, China*
[7]*Physical and Nuclear Energy and Engineering, Beihang University, Beijing 100191, China*

(Received 19 October 2023; accepted 23 February 2024; published 15 March 2024)

The lifetimes of the first 2^+ states in ^{116,118}Te were measured by means of the recoil distance Doppler-shift technique with the CIAE-plunger coupled to a HPGe array via ^{107}Ag(^{12}C, $3n$) and ^{110}Pd(^{12}C, $p3n$) reactions, respectively. The spectra are analyzed using the differential decay curve method. An improved precision for the lifetime of the 2_1^+ state in ^{118}Te was obtained, $\tau(2_1^+) = 8.2(5)$ ps, as well as a first measurement of the 2_1^+ state in ^{116}Te, $\tau(2_1^+) = 5.1(3)$ ps. The lifetime values complete the systematic data near midshell and contribute to the understanding of how quadrupole collectivity evolves in this mass region. The resulting $B(E2, 0_1^+ \rightarrow 2_1^+)$ transitions strength are discussed in relation to the systematics of the previously reported $B(E2, 0_1^+ \rightarrow 2_1^+)$ values in the Te isotopes and compared to the predictions of several models.

DOI: 10.1103/PhysRevC.109.034310

I. INTRODUCTION

The semimagic Sn ($Z = 50$) isotopes have been regarded as excellent examples of pairing dominance for decades based on the rather constant excitation energies of the 2_1^+ and 4_1^+ states, showing the typical features of seniority schemes. Recently, the advent of large-scale radioactive beam facilities and new detection technologies have enabled the study of the spectroscopy and transition properties of $N \approx Z$ nuclei just above the presumed doubly magic nucleus ^{100}Sn. Several unexpected phenomena have been observed: Large $B(E2, 0_1^+ \rightarrow 2_1^+)$ reduced transition probabilities remain almost constant for the $56 \leqslant N \leqslant 64$ Sn nuclei [1–8], instead of following the parabolic trend expected for the pairing domination. These unexpected results have given rise to various speculations [2,9–19]. An alternative explanation was offered by the Monte Carlo shell model calculations [16] performed in the full *gds* model space complemented by the $1h_{11/2}$, $2f_{7/2}$, and $3p_{3/2}$ orbitals for protons and neutrons. These calculations provided good reproduction of all measured $B(E2, 0_1^+ \rightarrow 2_1^+)$ values in the Sn chain and attributed their enhancement for $^{108-114}$Sn to the development of quadrupole deformation driven by proton core excitations from the $1g_{9/2}$ orbital. Very recently, these observations have been discussed in the context of pseudo-SU(3) symmetry acting in the space of *gds* orbitals excluding $1g_{9/2}$ [6,17]. They successfully reproduced the evolution of the $B(E2, 0_1^+ \rightarrow 2_1^+)$ values in $^{104-114}$Sn and demonstrated that modifications of the pairing strength had a negligible effect on the calculated $B(E2, 0_1^+ \rightarrow 2_1^+)$ values, in contrast to what was observed for the $B(E2, 2_1^+ \rightarrow 4_1^+)$ strengths.

The Te isotopes, which have only two protons in the $Z = 50$ shell, are expected to present features similar to those found for the Sn nuclei. Indeed, the experimental level energy systematics of the 2^+ and 4^+ states in neutron-deficient Te nuclei (shown in Fig. 1) display similar trends in the Sn and Te isotopic chains. Let us follow the evolution of the Te isotopes, starting at the top of the $N = 50$–82 neutron shell, towards the $N = 50$ shell closure. The closed neutron shell nucleus ^{134}Te exhibits the characteristic features of a rigid spherical system with a high 2^+ energy and a small $E(4^+)/E(2^+)$ ratio. As expected, the signatures of collectivity develop and become stronger with decreasing N. The 2^+ and 4^+ states minimise their energies in ^{120}Te ($N = 68$) near the neutron midshell ($N = 66$). As the neutron number is decreased further, below $N = 68$, the energies of the first excited 2^+ states stay essentially constant and show little influence of the $N = 50$ gap.

$E(2_1^+)$ energies are valuable indicators of nuclear deformation and collectivity as demonstrated by the well-known existence of a general systematic relationship between the transition strengths and the 2^+ energies according to global best fits in Refs. [22,23]. As expected, the signatures of collectivity develop and become stronger with decreasing N towards near midshell, where the 2^+ energy assumes a minimum value and the $B(E2, 0_1^+ \rightarrow 2_1^+)$ value reaches a maxima at $N = 68$.

*Corresponding author: licb@ciae.ac.cn

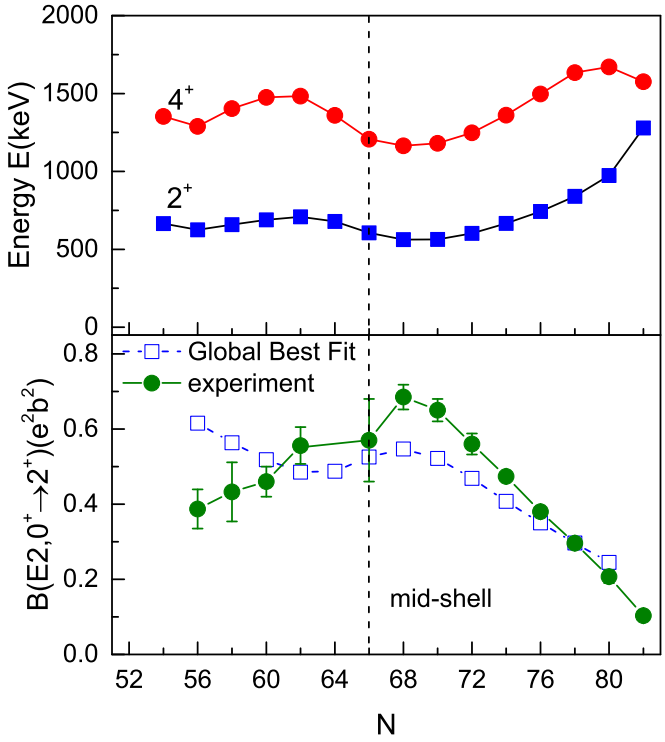

FIG. 1. Top panel: Systematics of 2^+ and 4^+ level energies for even mass Te isotopes; Bottom panel: Systematics of $B(E2, 0_1^+ \rightarrow 2_1^+)$ values for even mass Te isotopes compared with empirical data (square) derived from experimental 2_1^+ energies according to the formula proposed by Pritychenko, Birch, and Singh [22]. The experimental data marked with circles are taken from Refs. [20,21]. The neutron midshell at $N = 66$ is marked with the dashed vertical line.

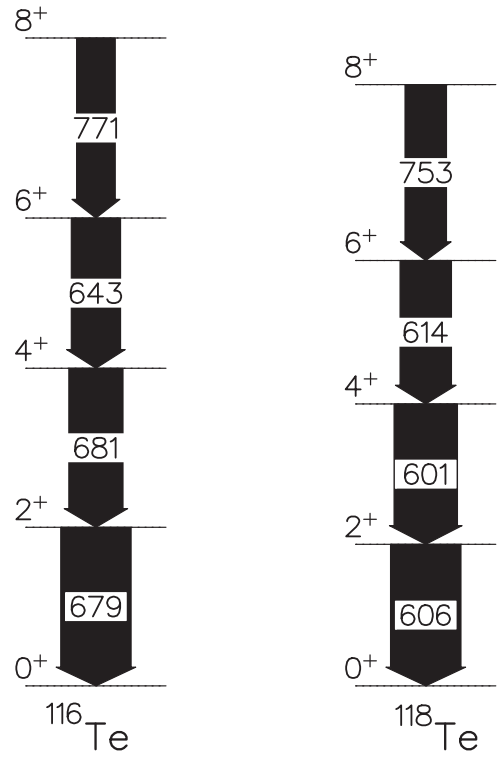

FIG. 2. Partial level schemes of ^{116,118}Te for the data analysis in the present study according to Refs. [31–33].

As the neutron number is decreased further, below $N = 68$, this trend is initially reversed with increasing 2^+ energies. An enhancement of transition probabilities is expected in Te isotopes for $N < 62$ (the empirical trend with global best fit shown in bottom panel of Fig. 1). However, the lifetime measurements of the 2_1^+ states in ^{108,110,112}Te clearly show that there has been no further increase in collectivity as a function of decreasing neutron number. Although several theoretical interpretations have been proposed for these unexpected results [24–30], the evolution of the $B(E2, 0_1^+ \rightarrow 2_1^+)$ values in the light Te nuclei remains puzzling. However, the absence of systematic data in ^{116}Te and the lack of precision in the literature for the $B(E2, 0_1^+ \rightarrow 2_1^+)$ value in ^{118}Te prohibits a definitive assignment of the trend, thus making further measurements in the vicinity of midshell $N = 66$ important.

Before the present experiment, no lifetime or $B(E2, 0_1^+ \rightarrow 2_1^+)$ value for ^{116}Te has been reported. Primarily, this is because the transitions from the 2^+ and 4^+ states in ^{116}Te form a doublet (see Fig. 2), which makes an analysis very difficult with any kind of measuring method. With the recoil-distance Doppler shift (RDDS) technique, only a very narrow gate width on the faster-velocity tail of the shifted component of the 681 keV, $4^+ \rightarrow 2^+$ transition at forward angle could be used to attain clean unshifted and shifted peaks for the 679 keV, $2^+ \rightarrow 0^+$ transitions, details on the data analysis are given in Sec. II. For ^{118}Te there is only one lifetime measurement with very large uncertainty [34]. In the present work we have, therefore, measured the lifetimes of the first excited 2^+ states in the tellurium isotopes ^{116,118}Te using the recoil-distance Doppler shift technique [35,36] to provide global and accurate data on the transition probabilities near the $N = 66$ midshell and shed more light on how quadrupole collectivity evolves in this mass region.

II. EXPERIMENTAL DETAILS AND RESULTS

The lifetime measurements of the present work were performed at the HI-13 tandem accelerator of the China Institute of Atomic Energy. The recoil distance Doppler-shift method was applied using the CIAE-plunger device [37–39] coupled to the Conjoint Gamma Array in China, which comprises 36 Compton-suppressed high-purity Ge detectors. The high-purity Ge detectors are grouped in five rings around the target. Nine of these detectors were placed at 90°, seven at 60°, eight at 120°, and six at 149° and 31° with respect to the beam direction. Two separate RDDS experiments were carried out using the ^{107}Ag(^{12}C, $3n$) ^{116}Te and ^{110}Pd(^{12}C, $p3n$) ^{118}Te reactions at beam energies of 57 and 64 MeV, respectively. Statistical model calculations with PACE4 were employed to determine the beam energies for the proper population. In the case of ^{116}Te, the target was enriched ^{107}Ag evaporated to a thickness of 0.9 mg/cm^2 onto a stretched 1.2 mg/cm^2 thick Au foil. For the ^{118}Te experiment, the target used was similarly prepared with enriched ^{110}Pd evaporated onto a 2.9 mg/cm^2 thick Al foil to a thickness of 0.76 mg/cm^2. A 10 mg/cm^2 Au foil

was used to stop the ^{116,118}Te recoil nuclei. The target and stopper foils were mounted in the CIAE-plunger with the Au/Al surface of the target foils facing the beam. The mean recoil velocities of the evaporation residues were ≈0.8% of the speed of light c for both experiments. The typical beam current was of the order of 2 pnA, limited by heating of the stretched target and the counting rate of the array. Eight target-to-stopper distances of 2 (the distance corresponding to electrical contact) to 40 μm for ^{116}Te and nine target-to-stopper distances of 2 to 90 μm for ^{118}Te were used to record RDDS data, and longer periods of beam time were spent on shorter distances in order to be sensitive to shorter lifetimes. Data at longer distances were also tentatively taken to investigate possible long-lived feeding into the states of interest. If one long-lived state dominantly feeds to the states of interest, no or a weak shifted component would be observed even for a large distance, which would hinder our measurements. In contrast, most of the transitions show a significant Doppler shifted component even for the short flight distance, indicating that there is no problem with dominant long-lived feeding into the 2^+ state. The distances were maintained by means of a piezoelectric device equipped with a feedback loop to check the stability of the plunger distances and regulate possible variations over time.

In order to determine lifetimes of the investigated levels, the differential decay curve method (DDCM) [40,41] was used in coincidence mode, avoiding the disturbing effects of sidefeeding. From the spectra gated on the shifted components of directly feeding γ transitions, we obtained the peak intensities of γ transitions depopulating the level of interest at different target-to-stopper distances x. The data of different target-stopper separations x have to be normalized to the corresponding number of nuclei produced at each separation x. The peak intensities acquired at different target-to-stopper distances were normalized by generating spectra with gates set on both the shifted and unshifted components of the $2^+ \rightarrow 0^+$ and $4^+ \rightarrow 2^+$ transitions. Then the summed intensities of the shifted and unshifted components of the higher lying transitions $6^+ \rightarrow 4^+$ and $8^+ \rightarrow 6^+$ were determined. It is known that the normalisation constants can be affected by the deorientation effect [36]. Thus, the sum of the total number of events in each coincidence matrix was used as a consistency check of the normalization procedure. The same normalization factors indicate a negligible effect. This may be caused by the detector angles of 31° and 149°, which are close to 55° and 125° where the Legendre polynomial of second order is close to zero and the angular distribution and correlation effects are weak. The lifetime $\tau(x)$ of the level of interest at each target-to-stopper distance x is obtained from

$$\tau(x) = \frac{\{B_s, A_u\}}{\frac{d}{dx}\{B_s, A_s\}} \cdot \frac{1}{v}, \tag{1}$$

where A stands for the depopulating transition and B for the direct feeding transition of the state of interest, and v denotes the recoil velocity. The quantities $\{B_s, A_u\}$ and $\{B_s, A_s\}$ denote the measured γ intensities of the depopulating transition A in coincidence with the shifted component of a populating transition B. The derivative, $\frac{d}{dx}\{B_s, A_s\}$, was determined by fitting piecewise continuously differentiable second order polynomials to the intensity values. In the ideal case, the derived values of $\tau(x)$ should not depend on the distance at which they have been determined and correspondingly should be a constant curve when plotted versus distance. Thus several independent lifetime values for a given level can provide a consistency check of the results and a deviation from such behavior immediately indicates the presence of systematic errors in the analysis. The determination of the lifetime by Eq. (1) was obtained by the program Napatau 2.0 [42].

By employing the direct gating described in the preceding paragraph, clean gated projection spectra were acquired, the examples of which are shown in Fig. 3 for the $2^+ \rightarrow 0^+$ transitions in ^{116,118}Te. As shown in this figure, the centroids of the stopped and flight components are well separated. The expected lifetimes of the first 2^+ states in ^{116,118}Te are of the order of a few or ten ps, which are far larger than the ions slowing-down time in the Au stopper (the order of 1 ps). Thus, the effects of the velocity distribution of the recoiling nuclei and the Doppler-shift attenuation occurring during the slowing down in the stopper were not taken into account. Such cases were treated according to the technique described in Ref. [43], where further details can be found. Finally, the intensities of these components could be approximatively determined by fitting two Gaussian peaks. It must be noted also that the gating region chosen for each of the determined lifetimes covers a part of the shifted component of the feeder. Events in the more shifted part of the peak correspond to faster recoils, whereas the γ rays emitted by the slower recoils appear less shifted. As a result, different gating regions correspond to different average velocities of the selected recoils. Therefore, the velocity was determined independently for each gate from the observed Doppler shift in the resulting cut spectrum.

Because of partial overlap between the shifted component of the 679 keV, $2^+ \rightarrow 0^+$ transition and the shifted component of the 681 keV, $4^+ \rightarrow 2^+$ transition in ^{116}Te, only a very narrow gate width on the faster-velocity tail of the shifted component of the 681 keV, $4^+ \rightarrow 2^+$ transition at forward angle 31° was used as shown in Fig. 4. Because the shifted component of the 681 keV, $4^+ \rightarrow 2^+$ transition is totally covered by the stopped and shifted component of the 679 keV ($2^+ \rightarrow 0^+$) transitions, the gates at backward angles detector rings can not be used. In the present work, six germanium detectors with excellent resolution were picked out from the forward-most ring at 31° for better distinguishing the shifted doublets. Notwithstanding, in this specific case, a blind gate on the spectrum will include the shifted component of the $2^+ \rightarrow 0^+$ transition. In order to achieve a clean gate, we simulated the relevant part of the spectrum by using Gaussians for the shifted and unshifted components of the known transitions in Fig. 4. The positions of the shifted components were fixed by using the Doppler formula and the experimentally determined mean recoil velocity. The widths of both the unshifted and shifted components were obtained from a width calibration, gained from the widths of uncontaminated peaks at different energies. Furthermore, in our data analysis, the gating regions used were checked for possible contaminations in the flight peaks arising from the overlap of the shifted

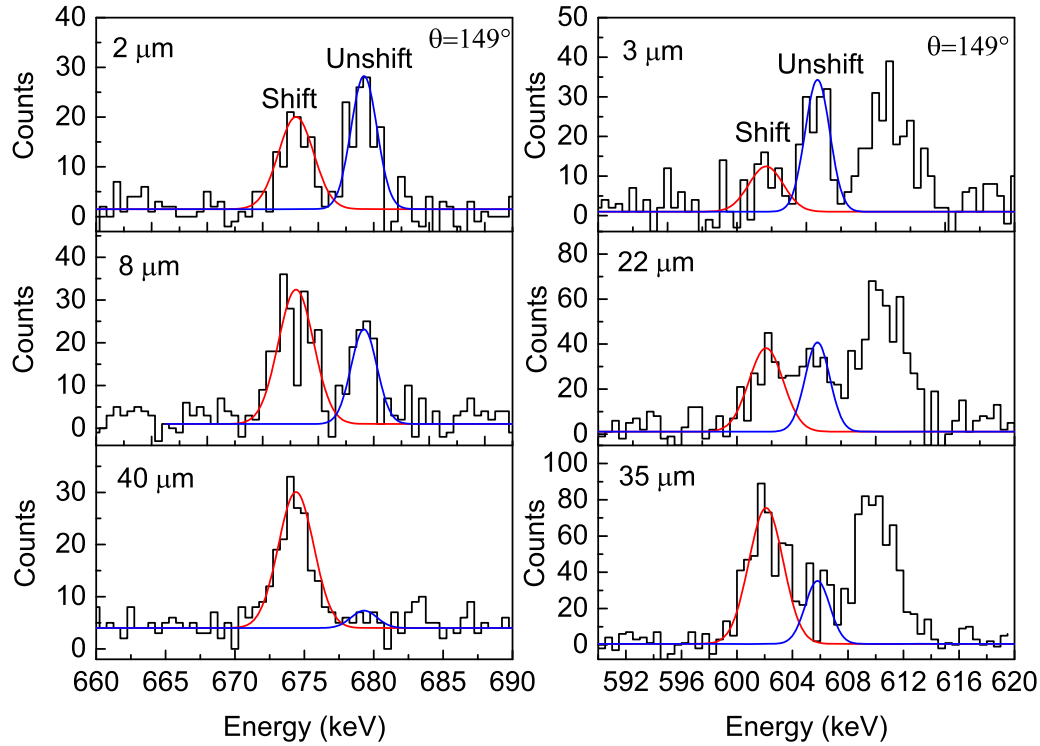

FIG. 3. Spectra of the $2^+ \rightarrow 0^+$ transitions in ^{116,118}Te at backward angle (149°) for three plunger distances. Left panel for ^{116}Te obtained by gating on the tail of the shifted component of the 681 keV (2 keV wide from 686 keV to 688 keV), $4^+ \rightarrow 2^+$ transition at forward angle 31°; right panel for ^{118}Te obtained by gating on the shifted component of the 601 keV (3.5 keV wide from 593 keV to 596.5 keV), $4^+ \rightarrow 2^+$ transition at backward angle 149°. The red and blue lines correspond to the shifted and unshifted components, respectively. The peak in the far-right of the right panel show the shifted component of the $6^+ \rightarrow 4^+$ transition.

component of the 679 keV ($2^+ \rightarrow 0^+$) transition. Four gate widths were placed on each transition depending on multipeak fitting as shown in Fig. 4 and the following results were checked for systematic deviations in the measured lifetime. In the instance where systematic deviations were observed,

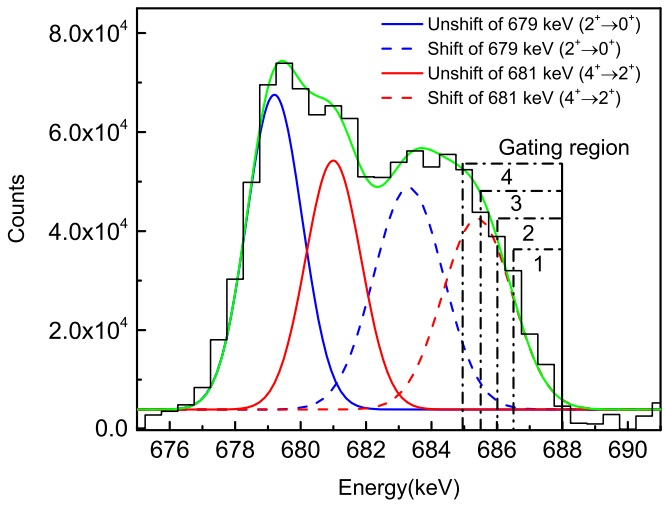

FIG. 4. Portion of the spectrum showing multipeaks of the $2^+ \rightarrow 0^+$, $4^+ \rightarrow 2^+$ transitions, and their shifted transitions at forward angle 31°. The histogram show the experimental data together with a fit function of four gaussian functions, as well as their decomposition.

the particular gating regions 3 and 4 were not included in the final analysis. Additionally, we determined two independent lifetime values from the analysis of the spectra of the two rings at different angles (31° and 149°), which were used to check for consistency. Due to the flight component of the γ ray being less shifted, the detector rings located at 60° and 120° were not used. The example of DDCM analysis for the $2^+ \rightarrow 0^+$ transition in ^{116}Te is shown in the left panels of Fig. 5. In the upper panel the τ curves are displayed, including the resulting lifetimes and their statistical errors. The middle and bottom panels depict the intensities of the shifted, and unshifted components, respectively, of the γ transitions of interest. The range of distances used for evaluating the mean τ is limited to the sensitive region of the measurement, where the numerator and denominator of Eq. (1) are not close to zero. The final value of the lifetime τ of the 2^+ of ^{116}Te was 5.1(3) ps by averaging the individual results. The deduced $B(E2, 0_1^+ \rightarrow 2_1^+)$ transition probability is 0.55(3) e^2b^2.

Lifetimes for the 2_1^+ state in ^{118}Te were determined by setting a direct gate on the Doppler-shifted component of the 601 keV, $4^+ \rightarrow 2^+$ transition at backward angle 149°. Due to overlap from the stopped component of the 606 keV, $2^+ \rightarrow 0^+$, the gates at forward angles detector rings were not used. At forward angles (shift to higher energies), the feeding transition of the unshifted component of the 614 keV($6^+ \rightarrow 4^+$ transition) partially overlaps with the shifted component of the 606 keV, $2^+ \rightarrow 0^+$ transition. However, as the 6^+ state was at higher excitation energies only a shifted component

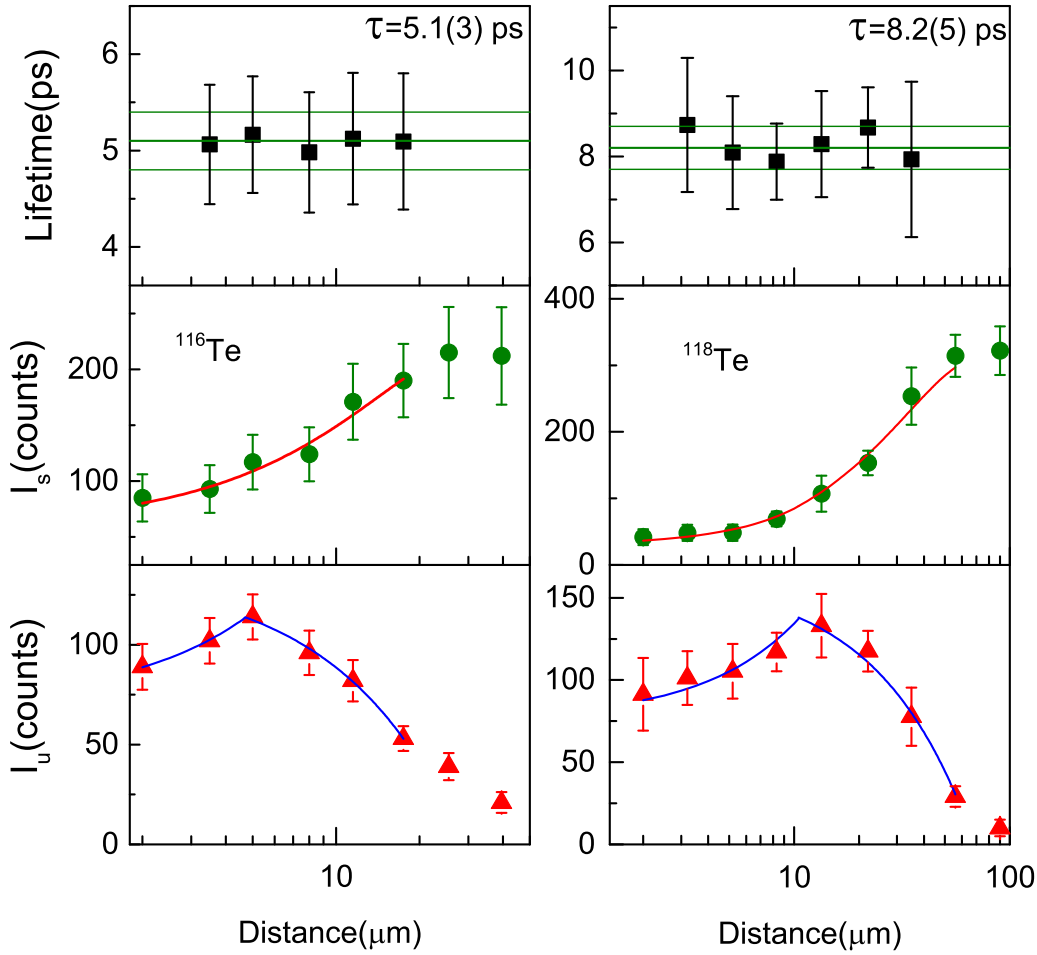

FIG. 5. DDCM analysis of 2_1^+ state in ^{116}Te (left) and the 2_1^+ state in ^{118}Te (right) gated by the direct feeders. In the upper panels the τ curves are displayed, including the resulting lifetimes and their statistical errors. The middle and bottom panels depict the intensities of the shifted and unshifted, respectively, components of the γ transitions of interest. See text for details.

can be visible in the spectrum, because the decay precedes the 4^+ and 2^+ transitions. This fact provides a sensitive check for remaining contaminant lines. From Fig. 6 it becomes evident that only a shifted component of the 614 keV, $6^+ \rightarrow 4^+$ transition was visible in the spectrum gated by the shifted component of the 601 keV, $4^+ \rightarrow 2^+$ transition. Thus, no such contaminated effects were observed. Mean lifetimes of 7.9(5) and 8.3(5) ps were determined for the backward-backward and backward-forward ring combinations, respectively. The coincidence decay curves and corresponding τ plot for the backward-backward combination are shown in the right panels of Fig. 5. The weighted mean value of these two lifetimes for the 2_1^+ state in ^{118}Te from the RDDS method is 8.2(5) ps, which agrees with the previous value $\tau = 8.8(14)$ ps obtained using the recoil distance Doppler shift attenuation method [34], however, with a much higher precision of the measurement. The deduced $B(E2, 0_1^+ \rightarrow 2_1^+)$ transition probability is 0.61(4) e^2b^2.

Due to overlap between shifted and/or unshifted components of $4^+ \rightarrow 2^+$ and $2^+ \rightarrow 0^+$ transitions in both ^{116,118}Te, the lifetime of the 4^+ states cannot be extracted via DDCM by gating on the shifted component of the $6^+ \rightarrow 4^+$ transition. In addition, due to poor statistics in the present experiment, levels at higher excitation energies and negative parity bands could not be analyzed either.

III. DISCUSSION

Experimental information on the $B(E2)$ systematics in Te isotopes based on the current measurement and Refs. [20,21] is presented in Fig. 7. Our newly measured $B(E2, 0_1^+ \rightarrow 2_1^+)$ values for ^{116,118}Te reveal a clear weakening of collectivity with decreasing N at midshell, which appears to shift the effective middle of the neutron shell towards $N = 68$–70, rather than displaying mirror symmetry about midshell. To understand the development of collectivity in the even-even Te chain and to help determine its nature, it is interesting to consider the Te data within regional systematics. Systematic $B(E2, 0_1^+ \rightarrow 2_1^+)$ transition rates for the $N = 64$, 66, and 68 isotones along with Z, as well for the Cd ($Z = 48$), and Sn ($Z = 50$) isotopic chains along with N are also shown in Fig. 7. In Fig. 7(a), the present results for ^{116}Te and ^{118}Te agree very well with expectations based on the systematics of $N = 64$, 66, and 68 isotones. The lack of symmetry about $Z = 50$ exhibited between Te and Cd, and other particle-hole nuclei can be explained as particle and hole excitations at the

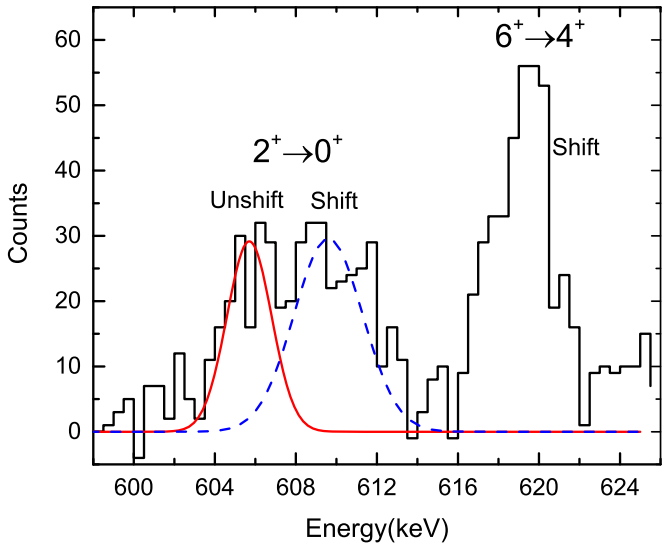

FIG. 6. Spectrum showing the $2^+ \rightarrow 0^+$ and $6^+ \rightarrow 4^+$ transitions in ^{118}Te at forward angle (31°) obtained by gating on the shifted component of the 601 keV, $4^+ \rightarrow 2^+$ transition at backward angle (149°). Because the decay has to happen before the compound nucleus stopped, only the shifted component of the $6^+ \rightarrow 4^+$ transition is visible in this spectrum.

beginning and at the end of the $Z = 50$ shell having different intrinsic structures. In addition, one notes in Fig. 7(b) that collectivity in tellurium is two to three times larger than for the Sn data. This can be understood in terms of two additional protons or holes in Te and Cd above/below the $Z = 50$ shell closure. It can be also noticed that, as the number of neutrons N increases, the Te and Cd isotopes follow similar paths. Contrary to what is observed in the Sn isotopes, the systematic $B(E2, 0_1^+ \rightarrow 2_1^+)$ values below the midshell ($N = 66$) show a significantly larger $B(E2, 0_1^+ \rightarrow 2_1^+)$ value compared to its heavier even-mass isotopes above the midshell. Between Cd and Te, many common features and phenomena have been observed experimentally along the isotopic chains [17,44–60]. In this context, the Te isotopes are expected to present properties similar to those found in their mirrored Cd isotopic chain.

In and near to shell closures, nuclear structure is determined by a compromise between the monopole part of the nuclear effective force that tends to stabilize the nucleus into a spherical shape, and the strong correlations dominated by pairing and quadrupole, in which quadrupole favors the nucleus into a deformed shape while pairing keeps the nuclear shape spherical [61,62]. As mentioned in the Introduction, the enhancement of $B(E2, 0_1^+ \rightarrow 2_1^+)$ values of neutron deficient semimagic Sn isotopes have triggered extensive studies for their physical mechanism in particular regarding the fundamental roles played by core excitations across the $Z = 50$ shell and the nuclear pairing correlation. Even though these two isotopic chains differ by only two protons, the Te and Sn nuclei present markedly different structures whose origin could be attributed to the enhanced proton-neutron interactions, which will influence the effective single-particle energies of the proton orbitals [63]. The effective single-particle energies depend on the proton-neutron effective interactions and the pairing properties [64]. The low-lying states carry a significant part of the proton single-particle strength for these isotopes. In addition, the collectivity in Te nuclei could be obtained in terms of the proton-neutron interaction generated by the two additional protons without any opening of the $Z = 50$ core [65]. Nonetheless, the clear presence of the proton $g_{9/2}$ intruder states in $Z \approx 50$ region suggests that the core excitations across the $Z = 50$ shell in Te nuclei may not be negligible for the low-lying structure [66,67]. The challenge to properly understand the role of proton core excitations remains. Moreover, from the neutron midshell on, the neutron $h_{11/2}$ orbital appears to introduce additional complexity since the attractive proton-neutron monopole interaction brings down the $h_{11/2}$ orbital which makes the neutrons more evenly distributed over the active orbitals [68,69]. The $B(E2, 0_1^+ \rightarrow 2_1^+)$ value is sensitive to details of shell structure. Thus, direct comparison between experimentally determined $B(E2, 0_1^+ \rightarrow 2_1^+)$ values and model predictions provides significant insight to microscopic origin.

First, in Fig. 8 we compare our results to large scale shell model (LSSM) calculations [29] using the CD-Bonn nucleon-nucleon potential, which was developed to reproduce well the spectroscopy of Te isotopes in full model valence space between the shell closures N (and Z) = 50 and 82 with a ^{100}Sn core. For $N, Z = 50$ the shell closure is complex and even the relative ordering of the $g_{7/2}$ and $d_{5/2}$ orbitals has been actively debated. Based on the assumption that the ground state of ^{105}Te has spin-parity $5/2^+$, the $g_{7/2}$ orbital was suggested to be the ground state of ^{101}Sn instead of $d_{5/2}$. In the LSSM calculations, the excitation energies were taken into account by setting $\epsilon_{sp}(g_{7/2}) = 0$ and $\epsilon_{sp}(d_{5/2}) = 0.172$ MeV. With the effective charge of $e_\pi = 1.5$ and $e_\nu = 0.8$ the LSSM predicts the experimental $B(E2, 0_1^+ \rightarrow 2_1^+)$ values for ^{116,118}Te measured in the present work remarkably well. However, the calculated $B(E2, 0_1^+ \rightarrow 2_1^+)$ values show a simple parabolic behavior, which do not break the symmetry about midshell. Thus the LSSM describes the overall agreement with experiment but it fails to describe the obvious reduction observed in collectivity from ^{120,122}Te to ^{118}Te at midshell.

Very recently, Kaneko *et al.* [18] performed an extended shell-model calculation taking into account a weakening of the $Z = 50$ shell closure with the quasi-SU(3) symmetry for even-even $^{108-134}$Te, showing an interesting deviation from the symmetric trend predicted by the seniority model. It is obvious from Fig. 8 that this breaking of the $Z = 50$ core gives an enhancement to the $E2$ transition probabilities in the midshell region, but, overestimates the data below midshell.

Recently, Sharma *et al.* [70] have performed a systematic study of even-even nuclei in the framework of a three-dimensional relativistic Hartree-Bogoliubov (RHB) model with density dependent meson exchange (DD-ME2) and point coupling (DD-PC1) as different effective interactions. They have predicted the values of β_2 and γ in the HFB energy minimum for $^{104-144}$Te isotopes. The resultant quadrupole deformation parameters (β_2) and triaxial parameters (γ) show prolate ground state minima for proton rich and neutron rich Te isotopes, oblate minima for $^{114-124}$Te, triaxial minima for ^{126,128}Te and spherical minima for $^{130-134}$Te. Additionally,

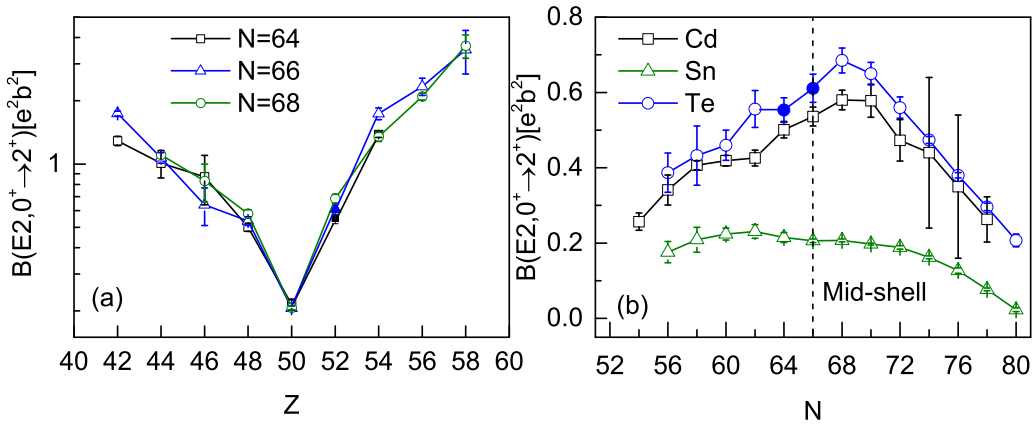

FIG. 7. (a) Systematic $B(E2, 0_1^+ \rightarrow 2_1^+)$ transition rates for the $N = 64$, 66, and 68 isotones. (b) Systematic $B(E2, 0_1^+ \rightarrow 2_1^+)$ transition rates for the Cd ($Z = 48$), Sn ($Z = 50$), and Te ($Z = 52$) isotopic chains. Open symbols are adopted and recently measured values from Refs. [20,21], while the values from this work for ^{116,118}Te is represented by the filled symbols.

oblate-prolate shape coexistence is predicted in $^{116-120}$Te isotopes.

The projected shell model (PSM) provides the framework in which the single-particle shell model can be applied to deformed nuclei. The predicted $B(E2)$ values are particularly sensitive to the quadrupole-quadrupole interaction, which is derived self-consistently with the β_2 parameter. Therefore, experimentally derived $B(E2, 0_1^+ \rightarrow 2_1^+)$ values are a valuable constraint to impose on the model. Calculated $B(E2, 0_1^+ \rightarrow 2_1^+)$s of the near midshell made with the projected shell model for $^{114-122}$Te [71] are also presented in Fig. 8. The oblate ground state deformations were taken in this study based on the above mentioned relativistic Hartree-Bogoliubov

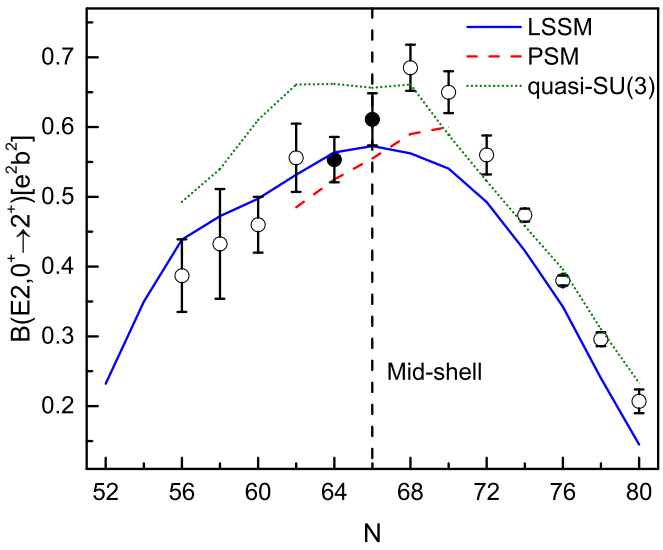

FIG. 8. Evolution of experimental $B(E2, 2_1^+ \rightarrow 0_1^+)$ values of even-even Te isotopes. The experimental results are compared with the recent LSSM (blue solid line) [29], PSM (red dash line) [71], and extend shell model with the quasi-SU(3) symmetry (green dotted line) [18] calculations. The open symbols are from Refs. [20,21] and closed symbols are from the current work.

mean field. The low-lying yrast and yrare states are reproduced well in these calculations. The experimental measured $B(E2, 0_1^+ \rightarrow 2_1^+)$ values for ^{116,118}Te in the present work are reproduced well. The weakening of collectivity with decreasing N is reproduced more satisfactorily near midshell in these calculations, which was suggested be related to the decrease in deformation, but a unified theoretical description of the Te isotopic chain is missing.

HFB calculations already suggested that oblate-prolate shape coexistence is predicted in $^{116-120}$Te isotopes and the $B(E2, 0_1^+ \rightarrow 2_1^+)$ trend could be altered by the calculations including a possibility of mixing of secondary prolate minima in PSM calculation with the generator coordinate method (GCM) [72,73]. Furthermore, in this $Z \approx 50$ region, Cd, Sn, and Te isotopes are often considered to be some of the best examples of shape coexistence involving particle-hole intruders [74–87]. These deformed intruder states, which are lowest in energy at midshell [75], are known to mix with the ground and first excited 2^+ states. This mixing could be partly responsible for the $B(E2, 0_1^+ \rightarrow 2_1^+)$ trends near midshell. Indeed, Rikovska *et al.* [66] considered a strong mixing between the normal vibration-like band and the deformed band built on intruder states. They showed by introducing the intruder configuration of the proton boson number $N_\pi = 3$ (note that the normal configuration is $N_\pi = 1$) that IBA-2 calculations taking into account mixing with an intruder $4p$-$2h$ configuration could improve the spectra and electromagnetic transition properties in $^{116-124}$Te. This elucidation can be placed in the context of shell model calculations with the quasi-SU(3) symmetry mentioned above, which show that breaking of the $Z = 50$ core can give an enhancement to the $E2$ matrix element for light Te isotopes. However, invoking core excitations alone does not resolve the $B(E2, 0_1^+ \rightarrow 2_1^+)$ discrepancies between theory and experiment. There is likely a rich mixture of physics occurring that will require many simultaneous ingredients such as possible $N = 64$ subshell effects [88–91], mass-dependent effective charges [14,15], and $s_{1/2}$ suppression of collectivity [2,9].

In addition, Raman *et al.* [92] have extensively compared the $B(E2, 0_1^+ \rightarrow 2_1^+)$ values for the Te isotopes with

different microscopic models, e.g., single-shell asymptotic Nilsson model, relativistic mean-field, Hartree-Fock calculations, and so on. However, none of these calculations appear capable of reproducing all of the features of the 2^+ transition strengths and clearly show the need for additional studies to firmly establish the nature of the low spin states in Te isotopes.

IV. SUMMARY

The current work presents lifetime measurements of the 2_1^+ states in ^{116,118}Te by means of the recoil distance Doppler-shift technique. The new lifetime of the 2_1^+ state in ^{116}Te complete the systematics of $B(E2, 0_1^+ \rightarrow 2_1^+)$ values near the neutron midshell. The measured 2_1^+ state lifetime with decreased uncertainty in ^{118}Te from this experiment is in good agreement with previous measurements. An obvious drop in $B(E2, 0_1^+ \rightarrow 2_1^+)$ systematics is observed at midshell $N = 66$, but is not reproduced so far by shell model calculations either excluding or including core excitations. In contrast with general shell model calculations, the deformed shell model approach with PSM, which unfortunately only have been performed for a segment of the major shell near midshell, suggests that the decrease in deformation may be responsible for the weakening trend of collectivity occurring from ^{120,122}Te to ^{118}Te. Furthermore, a rich mixture of physics involving shape coexistence and core excitations, possible $N = 64$ subshell effects, mass-dependent effective charges, and $s_{1/2}$ suppression of collectivity may all contribute to the observed overall $B(E2, 0_1^+ \rightarrow 2_1^+)$ trend in Te isotopes and their roles need to be investigated in the future.

While the measurement of $B(E2, 0_1^+ \rightarrow 2_1^+)$ values is very useful to investigate the evolution of collectivity along isotopic or isotonic chains, more insight into the collective behavior of a given nucleus can be gained from measuring the lifetimes of higher-lying states. For Te isotopes the yrast spectra show a vibrational-like equally spaced pattern, but the few known $E2$ transitions show that the Te isotopes may not be dominated by vibration but by other kinds of correlation. Hitherto, the experimental data for Te nuclei, especially for higher lying states, are scarce. Although the main focus of this work was determining the lifetime of the 2^+ state, further lifetime measurements to delineate the yrast band structures to higher spin and the nonyrast band are required to gain a more complete understanding of all the features in Te isotopes.

ACKNOWLEDGMENTS

We would like to thank the HI-13 tandem accelerator staff for the smooth operation of the machine. We are grateful to Dr. Q. W. Fan for their assistance during target preparation. This work is partially supported by the National Natural Science Foundation of China under Contract No. 11975315, No. U1932209, No. U2167202, and No. U2167201; and supported by the Leading Innovation Project of the CNNC under Grant No. LC202309000201.

[1] A. Ekström, J. Cederkäll, C. Fahlander, M. Hjorth-Jensen, F. Ames, P. A. Butler *et al.*, Phys. Rev. Lett. **101**, 012502 (2008).
[2] A. Jungclaus, J. Walker, J. Leske *et al.*, Phys. Lett. B **695**, 110 (2011).
[3] A. Banu, J. Gerl, C. Fahlander, M. Gorska, H. Grawe, T. R. Saito *et al.*, Phys. Rev. C **72**, 061305(R) (2005).
[4] J. Cederkäll, A. Ekström, C. Fahlander, A. M. Hurst, M. Hjorth-Jensen, F. Ames *et al.*, Phys. Rev. Lett. **98**, 172501 (2007).
[5] C. Vaman, C. Andreoiu, D. Bazin, A. Becerril, B. A. Brown, C. M. Campbell *et al.*, Phys. Rev. Lett. **99**, 162501 (2007).
[6] M. Siciliano, J. J. Valiente-Dobón, A. Goasduff *et al.*, Phys. Lett. B **806**, 135474 (2020).
[7] A. Corsi, S. Boissinot, A. Obertelli *et al.*, Phys. Lett. B **743**, 451 (2015).
[8] A. Kundu, M. S. R. Laskar, R. Palit, R. Raut, S. Santra, N. Shimizu *et al.*, Phys. Rev. C **103**, 034315 (2021).
[9] I. O. Morales, P. Van Isacker, and I. Talmi, Phys. Lett. B **703**, 606 (2011).
[10] T. Bäck, C. Qi, B. Cederwall, R. Liotta, F. Ghazi Moradi, A. Johnson, R. Wyss, and R. Wadsworth, Phys. Rev. C **87**, 031306(R) (2013).
[11] J. M. Allmond, A. E. Stuchbery, A. Galindo-Uribarri, E. Padilla-Rodal, D. C. Radford, J. C. Batchelder *et al.*, Phys. Rev. C **92**, 041303(R) (2015).
[12] L. Coraggio, A. Covello, A. Gargano, N. Itaco, and T. T. S. Kuo, Phys. Rev. C **91**, 041301(R) (2015).
[13] G. J. Kumbartzki, N. Benczer-Koller, K. H. Speidel, D. A. Torres, J. M. Allmond, P. Fallon *et al.*, Phys. Rev. C **93**, 044316 (2016).
[14] H. Jiang, Y. Lei, G. J. Fu, Y. M. Zhao, and A. Arima, Phys. Rev. C **86**, 054304 (2012).
[15] P. Doornenbal, S. Takeuchi, N. Aoi, M. Matsushita, A. Obertelli, D. Steppenbeck *et al.*, Phys. Rev. C **90**, 061302(R) (2014).
[16] T. Togashi, Y. Tsunoda, T. Otsuka, N. Shimizu, and M. Honma, Phys. Rev. Lett. **121**, 062501 (2018).
[17] A. P. Zuker, Phys. Rev. C **103**, 024322 (2021).
[18] K. Kaneko, N. Shimizu, T. Mizusaki, and Y. Sun, Phys. Rev. C **103**, L021301 (2021).
[19] N. Lo Iudice, Ch. Stoyanov, and D. Tarpanov, Phys. Rev. C **84**, 044314 (2011).
[20] B. Pritychenko, M. Birch, B. Singh, and M. Horoi, At. Data Nucl. Data Tables **107**, 1 (2016).
[21] D. A. Testov, S. Bakes, J. J. Valiente-Dobón, A. Goasduff, S. Frauendorf, F. Nowacki *et al.*, Phys. Rev. C **103**, 044321 (2021).
[22] B. Pritychenko, M. Birch, and B. Singh, Nucl. Phys. A **962**, 73 (2017).
[23] L. Grodzins, Phys. Lett. **2**, 88 (1962).
[24] B. Hadinia, B. Cederwall, J. Blomqvist, E. Ganioğlu, P. T. Greenlees, K. Andgren *et al.*, Phys. Rev. C **72**, 041303(R) (2005).
[25] D. S. Delion and V. V. Baran, AIP Conf. Proc. **1852**, 020002 (2017).
[26] B. Maheshwari, H. A. Kassim, N. Yusof, and A. K. Jain, Nucl. Phys. A **992**, 121619 (2019).

[27] T. Bäck, C. Qi, F. Ghazi Moradi, B. Cederwall, A. Johnson, R. Liotta *et al.*, Phys. Rev. C **84**, 041306(R) (2011).
[28] M. Doncel, T. Bäck, D. M. Cullen, D. Hodge, C. Qi, B. Cederwall *et al.*, Phys. Rev. C **91**, 061304(R) (2015).
[29] C. Qi, Phys. Rev. C **94**, 034310 (2016).
[30] S. Sharma, R. Devi, and S. K. Khosa, Chin. J. Phys. **66**, 474 (2020).
[31] A. Sharma, J. Singh, H. Kaur, J. Goswamy, N. Singh, and P. N. Trehan, Z. Phys. A **354**, 347 (1996).
[32] J. M. Sears, D. B. Fossan, I. Thorslund *et al.*, Phys. Rev. C **55**, 2290 (1997).
[33] C. B. Moon, T. Komatsubara, T. Shizuma *et al.*, Z. Phys. A **358**, 373 (1997).
[34] A. A. Pasternak, J. Srebrny, A. D. Efimov *et al.*, Eur. Phys. J. A **13**, 435 (2002).
[35] T. K. Alexander and J. S. Forster, Adv. Nucl. Phys. **10**, 197 (1978).
[36] A. Dewald, O. Möller, and P. Petkov, Prog. Part. Nucl. Phys. **67**, 786 (2012).
[37] J. L. Wang, X. G. Wu, C. Y. He *et al.*, Chin. Phys. C **38**, 036201 (2014).
[38] Q. M. Chen, X. G. Wu, Y. S. Chen *et al.*, Phys. Rev. C **93**, 044310 (2016).
[39] C. B. Li, H. L. Ma, X. G. Wu *et al.*, Phys. Rev. C **94**, 044307 (2016).
[40] A. Dewald, S. Harissopoulos, and P. von Brentano, Z. Phys. A **334**, 163 (1989).
[41] G. Böhm, A. Dewald, P. Petkov, and P. von Brentano, Nucl. Instrum. Methods Phys. Res. A **329**, 248 (1993).
[42] T. Pissulla, Ph.D thesis, University of Cologne, 2013.
[43] P. Petkov, D. Tonev, J. Gableske, A. Dewald, T. Klemme, and P. von Brentano, Nucl. Instrum. Methods Phys. Res. A **431**, 208 (1999).
[44] P. E. Garrett, K. L. Green, and J. L. Wood, Phys. Rev. C **78**, 044307 (2008).
[45] T. Schmidt, K. L. G. Heyde, A. Blazhev, and J. Jolie, Phys. Rev. C **96**, 014302 (2017).
[46] T. J. Gray, J. M. Allmond, and R. V. F. Janssens *et al.*, Phys. Lett. B **834**, 137446 (2022).
[47] M. Siciliano, J. J. Valiente-Dobón, A. Goasduff, T. R. Rodríguez, D. Bazzacco, G. Benzoni *et al.*, Phys. Rev. C **104**, 034320 (2021).
[48] M. Doncel, T. Bäck, C. Qi, D. M. Cullen, D. Hodge, B. Cederwall *et al.*, Phys. Rev. C **96**, 051304(R) (2017).
[49] D. S. Delion, R. Wyss, R. J. Liotta, Bo Cederwall, A. Johnson, and M. Sandzelius, Phys. Rev. C **82**, 024307 (2010).
[50] M. Saxena, Napiorkowski, R. Kumar *et al.*, Acta Phys. Pol. B **49**, 541 (2018).
[51] S. Pascu, N. V. Zamfir, Gh. Căta-Danil, and N. Mărginean, Phys. Rev. C **81**, 054321 (2010).
[52] B. Moon, C. B. Moon, P. A. Söderström, A. Odahara, R. Lozeva, B. Hong *et al.*, Phys. Rev. C **95**, 044322 (2017).
[53] Z. Y. Wu, C. Qi, R. Wyss, and H. L. Liu, Phys. Rev. C **92**, 024306 (2015).
[54] S. F. Hicks, J. R. Vanhoy, P. G. Burkett, B. R. Champine, S. J. Etzkorn, P. E. Garrett, S. W. Yates, and M. Yeh, Phys. Rev. C **95**, 034322 (2017).
[55] M. Saxena, Napiorkowski, L. Próchniak *et al.*, Acta Phys. Pol. B **50**, 417 (2019).
[56] B. J. Coombes, A. E. Stuchbery, J. M. Allmond *et al.*, EPJ Web Conf. **232**, 04003 (2020).
[57] S. Sharma, R. Devi, and S. K. Khosa, Phys. Rev. C **103**, 064312 (2021).
[58] K. Wrzosek-Lipska, L. Próchniak, P. E. Garrett *et al.*, Acta Phys. Pol. B **51**, 789 (2020).
[59] R. Devi and S. K. Khosa, Z. Phys. A **354**, 45 (1996).
[60] N. Boelaert, A. Dewald, C. Fransen, J. Jolie, A. Linnemann, B. Melon, O. Möller, N. Smirnova, and K. Heyde, Phys. Rev. C **75**, 054311 (2007).
[61] P. Federman and S. Pittel, Phys. Rev. C **20**, 820 (1979).
[62] T. Otsuka, A. Gade, O. Sorlin, T. Suzuki, and Y. Utsuno, Rev. Mod. Phys. **92**, 015002 (2020).
[63] T. Otsuka, R. Fujimoto, Y. Utsuno, B. A. Brown, M. Honma, and T. Mizusaki, Phys. Rev. Lett. **87**, 082502 (2001).
[64] N. A. Smirnova, A. De Maesschalck, A. Van Dyck, and K. Heyde, Phys. Rev. C **69**, 044306 (2004).
[65] R. F. Casten, Nucl. Phys. A **443**, 1 (1985).
[66] J. Rikovska, N. J. Stone, P. M. Walker, and W. B. Walters, Nucl. Phys. A **505**, 145 (1989).
[67] K. Heyde and J. L. Wood, Rev. Mod. Phys. **83**, 1467 (2011).
[68] F. Andreozzi, L. Coraggio, A. Covello, A. Gargano, and A. Porrino, Z. Phys. A **354**, 253 (1996).
[69] D. Bonatsos, K. E. Karakatsanis, A. Martinou, T. J. Mertzimekis, and N. Minkov, Phys. Rev. C **106**, 044323 (2022).
[70] S. Sharma, R. Devi, and S. K. Khosa, Nucl. Phys. A **988**, 9 (2019).
[71] S. Sharma, R. Devi, and S. K. Khosa, Int. J. Mod. Phys. E **31**, 2250053 (2022).
[72] F. Q. Chen, Y. Sun, and P. Ring, Phys. Rev. C **88**, 014315 (2013).
[73] C. B. Li, F. Q. Chen, X. G. Wu, C. Y. He, Y. Zheng, G. S. Li *et al.*, Phys. Rev. C **90**, 047302 (2014).
[74] M. Délèze, S. Drissi, J. Kern *et al.*, Nucl. Phys. A **551**, 269 (1993).
[75] P. E. Garrett, J. Phys. G: Nucl. Part. Phys. **43**, 084002 (2016).
[76] P. E. Garrett, T. R. Rodríguez, A. D. Varela, K. L. Green, J. Bangay, A. Finlay *et al.*, Phys. Rev. Lett. **123**, 142502 (2019).
[77] P. E. Garrett, T. R. Rodríguez, A. Diaz Varela, K. L. Green, J. Bangay, A. Finlay *et al.*, Phys. Rev. C **101**, 044302 (2020).
[78] S. F. Hicks, J. R. Vanhoy, and S. W. Yates, Phys. Rev. C **78**, 054320 (2008).
[79] D. Bonatsos, A. Martinou, S. K. Peroulis, and T. J. Mertzimekis, Atoms **11**, 117 (2023).
[80] M. Rastgar, H. Sabri, and A. O. Ezzati, Nucl. Phys. A **1039**, 122737 (2023).
[81] K. Kaneko, Y. Sun, N. Shimizu, and T. Mizusaki, Phys. Rev. Lett. **130**, 052501 (2023).
[82] J. B. Gupta, Phys. Rev. C **107**, 034315 (2023).
[83] H. Sabri, Z. Jahangiri, and M. A. Mohammadi, Nucl. Phys. A **946**, 11 (2016).
[84] T. Song and L. M. Yang, Phys. Rev. C **40**, 1782 (1989).
[85] P. E. Garrett, M. Zielińska, and E. Clément, Prog. Part. Nucl. Phys. **124**, 103931 (2022).
[86] S. F. Hicks, G. K. Alexander, C. A. Aubin *et al.*, Phys. Rev. C **71**, 034307 (2005).

[87] A. K. Singh, G. Gangopadhyay, and D. Banerjee, Phys. Rev. C **55**, 968 (1997).
[88] J. K. Hwang, A. V. Ramayya, J. H. Hamilton, Y. X. Luo, A. V. Daniel, G. M. Ter-Akopian, J. D. Cole, and S. J. Zhu, Phys. Rev. C **73**, 044316 (2006).
[89] V. R. Green, N. J. Stone, T. L. Shaw *et al.*, Phys. Lett. B **173**, 115 (1986).
[90] H. Hua, C. Y. Wu, D. Cline *et al.*, Phys. Rev. C **69**, 014317 (2004).
[91] T. Sumikama, K. Yoshinaga, H. Watanabe, S. Nishimura, Y. Miyashita, K. Yamaguchi *et al.*, Phys. Rev. Lett. **106**, 202501 (2011).
[92] S. Raman, C. W. Nestor, Jr., and P. Tikkanen, At. Data Nucl. Data Tables **78**, 1 (2001).